Numerical and stability analysis of Cu-Al_2O_3 water based hybrid nanofluid through a permeable shrinking sheet: Multiple solutions

Ali M. Mahnashi[1], Zeeshan[2*], Mohammad Alqudah[3], Naveed Iqbal[4], Rasool Shah[5]

[1]Department of Mathematics, Faculty of Science, Jazan University, P.O. Box 2097, Jazan 45142, Kingdom of Saudi .Arabia; ali.m@ju.edu.sa

[2]Department of Mathematics and Statistics Bacha Khan University Charsadda, KP, Pakistan

[3]Department of Basic Sciences, School of Electrical Engineering & Information Technology,

German Jordanian University, Amman, 11180, Jordan, mohammadquda@gju.edu.jo

[4]Deparment of Mathematics, College of Science, University of Ha'il, Ha'il 2440, Saudi Arabia; n.iqbal@uoh.edu.sa

[5]Department of Mathematics, Abdul Wali Khan University Mardan, Mardan, KP, Pakistan

*****Corresponding email**:** zeeshan@bkuc.edu.

Abstract

The aim of the current study is to investigate the numerical and theoretical analysis of hybrid nanofluid (NF)-suspended Cu and Al_2O_3 nanoparticles in water. The basic flow equations contain the influence of thermal radiation, magnetic field, temperature-dependent viscosity, cross-diffusion, and heat source. The basic flow equations described by Navier-Stokes have been altered to self-similar equations via transformations of variables. The transformed system is then solved numerically via the BVP4C approach. For stability exploration, the stability analysis is performed via mathematically and graphically which provides a novel contribution to the study. The impact of emerging factors on flow characteristics is elaborated through graphs. The present numerical results are correlated to the published work, and excellent agreement has been established. It is investigated that the velocity curves show decreasing phenomena due to the augmented values of variable viscosity and magnetic field. Opposite behavior is reported for the permeability factor, Grashof, and modified Grashof numbers. The fluid energy and concentration are increasing functions of the Dufour, Eckert, and Soret numbers.

Keywords: Numerical solution; Two branches solutions; Cross-diffusion; Grashof and Modified Grashof numbers effect; Lorentz force.

1. Introduction

Mechanical performance and material choices are significantly impacted by the transmission of heat. In the fields of medical study, the mechanisms of metabolism heat production, blood transport, capillaries dehydration, thermal management, and bio-heat exchanging routes make clear the significance of peristaltic fluid movement in heat transmission. All technological and biological structures generate heat, which causes a progressive decline in their ability to function. For such a device to function well, heat must be regularly evacuated from its construction. Novel materials having the ability to regulate heat transport are called nanofluids (NFs). The process that is employed to turn regular fluids into NFs is called nanoprecipitation. Etemad et al. [1] looked at the turbulent dynamics of NFs with thermal convection analysis. Beg and Tripathi [2] elucidated the peristaltic flow caused by the cross-diffusion of NFs pursuant to the influence of the Lorentz force. Beg et al. [3] analysed the NF in a permeability medium using an analytical technique. The computational models of NF across a vertical porous plate were provided by Ran et al. [4]. Convective boundary scenarios within a channel with porous walls have been used to find HAM-based conclusions for the NF [5]. The NF boundary layer mobility along an upward channel was explored by Rashidi et al. [6], and the method of homotopy analysis was used to get a quantitative result.

Hybrid nanofluids (HNFs) are a novel and exciting class of aqueous fluids that have garnered a lot of interest since they can alter their thermophysical characteristics to boost HT. This is realized by mixing a number of nano-additives to fulfill the unique desires of every use. HNFs can be used in solar energy, electrical wiring, cooling structures, heat transfer devices, and heat tunnels. Muneeshwaran et al. [7] outlined the character of HNF in heat diffusion, although Kshirsagar and Co. [8] decorated the wide range of technical uses for it. For solar systems, researchers have reported on the thermal and mixture features of HNF [9, 10]. Esfe et al. [11] anticipated that HNF would be used in machining processes. Applications of HNFs with heat capacity were described by Adun et al. [12]. For the heat transfer rate, numerical findings were produced, and a visual representation of the physical components' influence on the flow field was provided. The HNF was looked at by Akilu et al. [13] to increase solar energy. In an analogous vein, Ashorynejad and Shahriari [14] examined the conduction of HNF over a wavy cavity when Lorentz force was present.

Most investigations involving MHD and NFs across stretched sheets typically include thermal fluidity or a constant wall temperature. Aziz [15] looked at the Blasius mobility across a stretched sheet under conduction heating conditions. Temini et al. [16] studied the numerical solution for Troesh's problem using Shishkin mesh. Ben-Romdhane et al. [17] reported the numerical solutions for boundary layer problem. Falkner-Skan flow problem was discussed by Temimi et al. [18]. Dual solutions for the 2D flow of Bratu's problem was displayed by Temimi et al. [19].

Comparably, Aziz and Khan [20] looked into the magnetized NF using a warmed vertical plate. Implications for chemical reactions have not been factored into these studies. Reaction is a crucial process in the processing of materials. The chemical reactions can be uniform, inconsistent, or endothermic. Kumar et al. [21] discussed the MHD movement with heat analysis of non-miscible micro polar fluid over rectangular permeable sheet. Yadav and Yadav [22] investigated the heat mass transmission of MHD couple-stress fluids over permeable curved framework. Yadav and Srivastava [23] reported the influence of slip and permeable material in MHD movement across an inclined framework. Similarly, Jaiswal and Yadav [24] examined the movement of micropolar-Newtonian liquids with porous effect in a movable interface. Yadav et al. [25] reported the Poiseuille flow in a permeable pipes of micropolar Newtonian fluid. Boundary-layered convection formulations incorporating chemical processes have been distributed [26]. Manjunatha et al. [27] examined the effects of cross-diffusion and chemical processes on magnetized heat transfer. They discovered that chemical reaction ordering increases concentrating boundary layer depth, but specie diffusion increases the adverse chemical response rate.

The investigation of the stability of the time-dependent viscosity of HNF over a stretching and contracting surface with the impact of heat radiation, chemical reactions, and cross-diffusion is novel in this work. This model is the extension of the models reported by Manjunatha et al. [27] and Venkateswarlu et al. [28]. Moreover, stability analysis has been implemented which is not investigated yet. Through similarity variables, the fundamental flow model expressed by means of partial differential equations (PDEs) altered to a non-dimensional version expressed in systems of ordinary differential equations (ODEs), and then cracked numerically. The outcomes are validated against the available outcomes. The theoretical examination's results may soon find use in a wide range of industries, including the manufacture of medical equipment, surfactants,

lubrication properties, hybrid power plants, solar heating and cooling technologies for automobiles, and metallurgical welding processes.

2. Mathematical analysis

In a porous medium comprising copper and alumina tiny particles, the two-dimensional movement of HNF is examined beneath the effects of heat radiation, chemical reactions, cross-diffusion, magnetic fields, and time-dependent viscosity. In this investigation, water is used as a host fluid. In Figure 1, the flow structure is illustrated. It is evident from the graphic that the flow is across the x-axis and the y-axis is normal to it. The extending/shrinking velocity is signified by $U_w = \lambda cx$, where λ is the stretching or shrinking parameter. The Lorentz force is occupied normal to the flow. Here, T_w, T_∞, C_w, and C signify the surface and ambient temperatures with surface, and ambient concentrations, separately.

The leading flow equations of velocity, temperature, and concentration are given below B_0

$$\frac{\partial}{\partial x}(u)+\frac{\partial}{\partial y}(v)=0, \tag{1}$$

$$\frac{1}{\rho_{hnf}}\left\{\frac{\partial}{\partial y}\left(\mu_{hnf}(T)\frac{\partial u}{\partial y}\right)-\left(\sigma B_0^2+\frac{\nu_f}{k_f}\right)u\right\}-\left\{u\frac{\partial u}{\partial x}+v\frac{\partial u}{\partial y}\right\}+g\beta_{hnf}\left\{\left(\mathrm{C}-C_\infty\right)+\left(T-T_\infty\right)\right\}=0, \tag{12}$$

$$\frac{1}{(\rho Cp)_{hnf}}\left\{(k_{hnf}+\frac{16\sigma^* T_\infty^3}{3\mathrm{k}^*})\frac{\partial^2 T}{\partial y^2}+Q^*\left(T-T_\infty\right)\begin{matrix}+Ql^*\left(C-C_\infty\right)+\\ \mu_{hnf}\left(\frac{\partial u}{\partial y}\right)^2\end{matrix}\right\}-\left\{u\frac{\partial T}{\partial x}+v\frac{\partial T}{\partial y}\right\} \tag{3}$$

$$+\frac{Dk_T\partial^2 C}{CpC_s\partial y^2}=0$$

$$D_B\frac{\partial^2 C}{\partial y^2}-\left\{u\frac{\partial C}{\partial x}+v\frac{\partial C}{\partial y}\right\}-K_r^*\left(C-C_\infty\right)+\frac{Dk_T}{T_m}\frac{\partial^2 T}{\partial y^2}=0. \tag{4}$$

With BCs

$$C=C_w, T=T_w, U_w=u=\lambda cx, and\ v=0 \text{ at } y=0,$$

$$C=C_\infty, T=T_\infty, u=0, and\ v=0 \text{ at } y\to\infty. \tag{5}$$

Tables 1 and 2 signify the thermo-physical properties of the proposed model.

Where $\frac{k_{bf}}{k_f} = \frac{k_{s1} + (n-1)\left\{k_f + \phi_2\left(k_{s1} - k_f\right)\right\}}{k_{s1} + (n-1)\left\{k_f + \phi_2\left(k_f - k_{s1}\right)\right\}}$.

For time-dependent viscosity, the following relation is used [27-29]:

$$\mu_f = \mu_0 e^{-B\theta(\eta)}. \tag{6}$$

The term $e^{-B\theta(\eta)}$ can be expand by utilizing Maclaurin's series

$$e^{-B\theta} = 1 - (B\theta) + O\left(B^2\right). \tag{7}$$

In terms of variable viscosity, HNF is reported as

$$\frac{\mu_f}{\left(1-\phi_1\right)^{2.5}\left(1-\phi_2\right)^{2.5}},$$

$$\mu_{hnf}(T) = \frac{\mu_0}{\left(1-\phi_1\right)^{2.5}\left(1-\phi_2\right)^{2.5}} \exp\{1 - B\theta(\eta)\}, \tag{8}$$

$$\frac{\mu_0}{(1-\phi_1)^{2.5}(1-\phi_2)^{2.5}} \exp\{1 - (B\theta) + O(B^2)\}.$$

In Eq. (8), B (for liquid $(B<0)$, for gasses $(B<0)$ is parameter depending on the viscosity of the fluid and $\mu_0$is the reference viscosity.

Using the transformation variable [27, 28]

$$u = axf'(\eta), v = -\sqrt{a*\nu_f}\, f(\eta), \theta(\eta) = \frac{T_\infty - T}{T_\infty - T_w}, \varphi(\eta) = \frac{C_\infty - C}{C_\infty - C_w}, \eta = \sqrt{\frac{a}{\nu_f}} * y. \tag{9}$$

In view of (9), equations (2)-(5) become

$$(1 - B\theta) f'' - A_2 A_1\left(f'^2 - f'' f\right) + A_3 A_2 A_1 (Gm\varphi + Gr\theta) - Bf''\theta' - A_1(1/K + M) f' = 0, \tag{10}$$

$$\frac{1}{\Pr}\left\{A_5 + \frac{4}{3}R\right\}\theta'' + A_4 f\theta' + Q\theta + Q1\phi + A_1 Ecf''^2 + A_4 Du\phi'' = 0, \tag{11}$$

$$\frac{1}{Sc}\varphi'' + f\varphi' - Kr\varphi + \mathrm{Sr}\theta' = 0. \tag{12}$$

With

$$f^{'} = \lambda, \theta = 1, \phi = 1, f = 0 \text{ at } \eta = 0,$$

$$f^{'} = 0, \theta = 0, \phi = 0 \text{ at } \eta \to \infty. \tag{13}$$

In above equations the parameters are given below

$$Gr = \frac{g\beta_f (T_w - T_\infty)}{aU_w}, Gm = \frac{g\beta_f (C_w - C_\infty)}{aU_w}, K = \frac{a(k\rho)_f}{\nu_f}, Kr = \frac{Kr^*}{a}, M = \frac{\sigma B_0^2}{a\rho_f},$$

$$Ec = \frac{u_w^2}{(C_p)_f (T_w - T_\infty)}, \Pr = \frac{\nu_f (\rho Cp)_f}{k_f}, \; R = \frac{4\sigma^* T_\infty^3}{k^* k_f}, Q = \frac{Q^*}{a(\rho Cp)_f}, Sc = \frac{\nu_f}{D_B},$$

$$Sr = \frac{Dk_T}{T_n \nu_f}\left(\frac{T_w - T_\infty}{C_w - C_\infty}\right), u = \frac{Dk_T}{C_p C_s \nu_f}\left(\frac{C_w}{T_w - C_\infty}\right), Q1 = \frac{Ql^*}{a(\rho C_p)_f}\left(\frac{C_w - C_\infty}{T_w - T_\infty}\right).$$

Dimensionless Local Skin Friction and Local Nusselt number are

$$S_f Re_x^{\frac{1}{2}} = -\frac{\mu_{hnf}}{\mu_f} f^{"}(0),$$

$$N_n^{-\frac{1}{2}} = -\frac{K_{hnf}}{K_f}\theta^{'}(0).$$

3. Numerical solution

Nonlinear ODEs (10)–(12) with constraints (13) cannot be analytically addressed. Computational methods are required to solve differential equations of this type. Although the available literature presents several numerical techniques, the bvp4c technique is mostly helpful for 1st-order initial value problem (IVP). Consequently, we solved the system (10)–(12) using the bvp4c method and the relevant constraint (13). The aforementioned equations are changed to the system of 1st-order by employing the alteration variables:

$$f = f_1, \frac{df}{d\eta} = f^{'} = f_2, \frac{d^2 f}{d\eta^2} = f^{"} = f_3, \theta = f_4, \frac{d\theta}{d\eta} = \theta' = f_5, \phi = f_6, \frac{d\varphi}{d\eta} = \phi^{'} = f_7. \tag{14}$$

Using (14) in (10)-(13), we have

$$f_3' = \frac{1}{1 - B\theta}\begin{Bmatrix} A_1 A_2\{(f_2^2 - f_1 f_3) - A_3(\mathrm{Gm}\ f_6 + Gr f_4)\} \\ + B f_3 f_5 + A_1\left(\frac{1}{K} + M\right) f_2 \end{Bmatrix}, \tag{15}$$

$$f_5' = -E^*\begin{Bmatrix} A_4 f_1 f_5 + Q f_4 + Ql f_6 + A_1 Ec f_3'^2 + A_4\,\mathrm{DuSc}(\mathrm{Kr}\, f_6 - f_1 f_7) \end{Bmatrix}, \tag{16}$$

$$f_7^{'} = -F^*\left\{ f_1 f_7 - Krf_6 - \frac{3PrSr}{A_5 + 4R}\left\{ A_4 f_1 f_5 + Qf_4 + Qlf_6 + A_1 Ecf_3^{"2} \right\} \right\}. \tag{17}$$

Corresponding to the conditions

$$f_{1a^*} = 0, f_{2a^*} = \lambda, f_{4a^*} = 1, f_{6a^*} = 1, \quad f_{2b^*} = \lambda, f_{4b^*} = 1, f_{6b^*} = 1. \tag{18}$$

where $E^* = -\dfrac{3Pr}{3A_5 + 4R - 3A_4 PrDuScSr}, F^* = -\dfrac{\left(A_5 + 4R\right)Sr}{A_5 + 4R - A_4 DuPrSCSr}$.

The set of equations (15)–(17) and the associated BCs provided by (18) can be addressed using the bvp4c method. Until the solution satisfies the convergence requirements, the process is repeated to confirm that the results satisfy the necessary accuracy level of 10^{-6}. In Fig. 2, the bvp4c structure is shown.

4. Stability analysis

Together with the shooting procedure, the resultant nonlinear ODEs are computed using the bvp4c method. For the purposes of this investigation, stability analysis is used since certain values show dual solutions. Stretching or shrinking the sheet leads to dual solutions. For this reason, finding a stable and physically possible stability analysis of the problem is important. The approach used for stability reasons is precisely the same as Dero et al. [30] was described. The unsteady flow equations are:

$$\frac{\partial}{\partial x}(u) + \frac{\partial}{\partial y}(v) = 0, \tag{19}$$

$$\begin{aligned} &\frac{\partial u}{\partial t} + \frac{1}{\rho_{hnf}}\left\{ \frac{\partial}{\partial y}\left(\mu_{hnf}(T)\frac{\partial u}{\partial y} \right) - \left(\sigma B_0^2 + \frac{\nu_f}{k_f} \right)u \right\} - \left\{ u\frac{\partial u}{\partial x} + v\frac{\partial u}{\partial y} \right\} \\ &+ g\beta_{hnf}\left\{ \left(\mathrm{C} - C_\infty \right) + \left(T - T_\infty \right) \right\} = 0, \end{aligned} \tag{20}$$

$$\begin{aligned} &\frac{\partial T}{\partial t} + \frac{1}{(\rho Cp)_{hnf}}\left\{ (k_{hnf} + \frac{16\sigma^* T_\infty^3}{3\mathrm{k}^*})\frac{\partial^2 T}{\partial y^2} + Q^*\left(T - T_\infty \right) \right. \\ &\left. + Ql^*\left(C - C_\infty \right) + \mu_{hnf}\left(\frac{\partial u}{\partial y} \right)^2 \right\} - \left\{ u\frac{\partial T}{\partial x} + v\frac{\partial T}{\partial y} \right\} + \frac{Dk_T \partial^2 C}{CpC_s \partial y^2} = 0 \end{aligned} \tag{21}$$

$$\frac{\partial C}{\partial t} + D_B\frac{\partial^2 C}{\partial y^2} - \left\{ u\frac{\partial C}{\partial x} + v\frac{\partial C}{\partial y} \right\} - K_r^*\left(C - C_\infty \right) + \frac{Dk_T}{T_m}\frac{\partial^2 T}{\partial y^2} = 0. \tag{22}$$

The corresponding boundary conditions (BCs) are

$$C = C_w, T = T_w, U_w = u = \lambda cx, and\, v = 0 \text{ at } y = 0,$$

$$C = C_\infty, T = T_\infty, u = 0, and\, v = 0 \text{ at } y \to \infty. \tag{23}$$

According to Dero et al. [30], the subsequent alterations of variables are presented to convert the unsteady PDEs (20)-(23) in terms of ODEs.

Using the transformation variable [30]

$$\begin{aligned} &u(x,t) = axf'(\eta,\Gamma), v(x,t) = -\sqrt{a*\nu_f}\, f(\eta,\Gamma), \theta(x,t) = \frac{T_\infty - T}{T_\infty - T_w}, \\ &\phi(x,t) = \frac{C_\infty - C}{C_\infty - C_w}, \eta = \sqrt{\frac{a}{\nu_f}} * y, \Gamma = ct. \end{aligned} \tag{24}$$

In view of Eq. (24), Eqs. (20)-(23) become

$$\begin{aligned} &(1 - B\theta)\frac{\partial^3 f}{\partial \eta^3} - A_2 A_1 \left(\left(\frac{\partial f}{\partial \eta} \right)^2 - \frac{\partial^2 f}{\partial \eta^2} f \right) + A_3 A_2 A_1 (Gm\varphi + Gr\theta) - B\frac{\partial^2 f}{\partial \eta^2}\frac{\partial \theta}{\partial \eta} - \\ &A_1 \left(\frac{1}{K} + M \right)\frac{\partial f}{\partial \eta} - \frac{\partial^2 f}{\partial \eta \partial \Gamma} = 0, \end{aligned} \tag{25}$$

$$\frac{1}{\Pr}\left\{ A_5 + \frac{4}{3}R \right\}\frac{\partial^2 \theta}{\partial \eta^2} + A_4 f\frac{\partial \theta}{\partial \eta} + Q\theta + Ql\phi + A_1 Ec\left(\frac{\partial^2 f}{\partial \eta^2} \right)^2 + A_4 Du\frac{\partial^2 \phi}{\partial \eta^2} - \frac{\partial^2 \theta}{\partial \eta \partial \Gamma} = 0, \tag{26}$$

$$\frac{1}{Sc}\frac{\partial^2 \phi}{\partial \eta^2} + f\frac{\partial \phi}{\partial \eta} - Kr\phi + Sr\frac{\partial \theta}{\partial \eta} - \frac{\partial \phi}{\partial \Gamma} = 0. \tag{27}$$

With

$$\begin{aligned} &\tfrac{\partial f}{\partial \eta}(\eta = 0, \Gamma) = \lambda, \theta(\eta = 0, \Gamma) = 1, \phi(\eta = 0, \Gamma) = 1, f(\eta = 0, \Gamma) = 0, \\ &\tfrac{\partial f}{\partial \eta}(\eta \to \infty, \Gamma) = 0, \theta(\eta \to \infty, \Gamma) = 0, \phi(\eta \to \infty, \Gamma) = 0. \end{aligned} \tag{28}$$

Rendering to Lund et al. [29], the reliability of the steady movement can be observed where $f_0(\eta) = f(\eta), \theta_0(\eta) = \theta(\eta)$ and $\phi_0(\eta) = \phi(\eta)$ which satisfy (10)-(13), i.e.,

$$\begin{aligned} &f(\eta,\Gamma) = f_0(\eta) + e^{-\gamma\Gamma} J(\eta,\Gamma), \\ &\theta(\eta,\Gamma) = \theta_0(\eta) + e^{-\gamma\Gamma} F(\eta,\Gamma), \\ &\phi(\eta,\Gamma) = \phi_0(\eta) + e^{-\gamma\Gamma} G(\eta,\Gamma). \end{aligned} \tag{29}$$

Where $J(\eta), F(\eta)$, and $G(\eta)$, are relatively small to $f_0(\eta), \theta_0(\eta)$, and $\phi_0(\eta)$ and γ is the eigenvalue (unknown). In view of (29), Eqs. (25)-(27), and taking $\Gamma = 0$.

$$(1-B\theta)J^{"} - A_2A_1\left(J^{'2} - J^{"}f_0\right) + A_3A_2A_1(Gm\varphi + Gr\theta) - BJ^{"}F^{'} - A_1(1/K + M)J^{'} + \gamma J = 0, \quad (30)$$

$$\frac{1}{\Pr}\left\{A_5 + \frac{4}{3}R\right\}F^{"} + A_4 f_0 F^{'} + Q\theta_0 + Ql\phi_0 + A_1 EcJ^{"2} + A_4 DuG^{"} + \gamma F = 0, \quad (31)$$

$$\frac{1}{Sc}G^{"} + f_0 G^{'} - Kr\phi_0 + \mathrm{Sr}F^{'} = 0. \quad (32)$$

With

$$J^{'} = \lambda, F = 1, \mathrm{G} = 1, J = 0 \text{ at } \eta = 0,,$$

$$J^{'} = 0, F = 0, \mathrm{G} = 0 \text{ at } \eta \to \infty. \quad (33)$$

According to [29, 30]. So, $J^{'} = 0$ at $\eta \to \infty$ will be taken as $J^{"}(0) = 1$.

5. Results and discussion

In this section, we shall examine the intriguing effects of several physical parameters of interest on flow dynamics. Additionally, we will discuss the engineering properties of mass movement rates, heat, and SF that are present in both conventional and HNF streams over a perforated sheet. The complicated set of problems (13)–(15) is solved numerically using the bvp4c approach, along with boundary conditions (16), and represented graphically.

The present investigated results are confirmed by comparing with the published study, as shown in Tables 3 and 4 below. Tables 3, 4 show that when $R = Q = Q1 = 0 = Du = Sc = Sr = Kr$, there is a strong correlation between the present findings and published [27, 28] for different values of $Ec = 0:3, Pr = 0.5, and\ Gr = B = 1.2$. Furthermore, it is clear from the table that as parameters $M, B,$ and Pr grow, so does the SDF and Nusselt number. Moreover, it is noteworthy that SDF and HT for Cu-Al_2O_3-H_20 is higher than Cu-H_20.

Theoretical and visual stability explorations are offered to determine the stable configuration that results from the contracting sheet. Figure 3 provides a graphical representation of the dual solutions. According to Dero et al. [30], solution is stable for positive eigenvalues and unstable for negative. The crucial point represents convergence where the Ist and 2nd branches meet. When there are several branches, the stability examination is heavily used to assess the stable branch.

The impact of B (vairable viscosity factor), M (magnetic factor), Gr (Grashof number), Du (Dufour number), Ec (Eckert number), Q (heat source) and $Q1$ (radiation absorption) on the skin friction (S_f) and Nusselt number $((N_n))$ is illustrated in Figures (4)-(10). Figures 4-6 demonstrate the changes in S_f for various values of B, M, and Gr, while graphs 7-10 scrutinize the inspiration of Du, Ec, Q, and $Q1$ on the fluctuation of (S_f). In Figure 4, it is depicted that as the amount of B, M growths, the value of S_f also increases. Notably, the parameters B and M exhibit dual fluctuation on (S_f). In the first branch, (S_f) experiences an increase, whereas in the second branch, (S_f) witnesses a decrease. This phenomenon can be ascribed to the presence of the Lorentz force, which arises from the magnetic field and opposes the flow, resulting in a decline in (S_f) during the second branch. The disparity in the amount of M on the variation of (S_f) is shown in Figure 5. The data reveals that as M increases from 1 to 3, (S_f) experiences an enhancement.

Similarly, as the value of B increases from 1 to 5, the parameter S also experiences a corresponding increase. The rise in S can be directly attributed to the increasing magnitudes of M, which range from 1 to 3. The reason behind this phenomenon lies in the resistive forces become more prominent and discernible within this range. The mixture of Cu and alumina-nanoparticles known as HNF, plays a crucial role in promoting an enhanced resistance to movement. This is primarily due to the higher surface area possessed by these nanoparticles and their amplified alliance with the liquid component.

The inspiration of Gr and M on (S_f) of HNF is illustrated in Figure 6. Interestingly, a duality behavior is observed in relation to these parameters. The term Gr pertains to the buoyancy forces involved in the fluid drive. Upon investigation, it is found that the value of (S_f) drops as the amounts of Gr and M are improved. This implies that as Gr and M values increase, the skin friction experienced by HNF decreases.

The occurrence of this inverse behavior can be attributed to the low resistance encountered during the movement, which can be primarily attributed to the increasing values of Gr. The rising level of Gr introduce a resilient fluid motion, thereby mitigating the resistance to stream and consequently leading to a decline in (S_f). Figures 7-9 present a comprehensive analysis of

the behavior of N_n and its dependence on the parametersDu, Ec, and Q for the HNF. Upon examining Figure 7, it is evident that as the value of the factor Du increases from 1 to 3, the HT of hybrid nanofluid losses. Notably, it is crucial to highlight that the heat percentage experiences an enhancement in the second branch. This same pattern can be detected for the Ec factor's influence onN_n, as depicted in Figure 8. By analyzing the mathematical appearance of Ec, it becomes evident that Ec exhibits a straight relationship with velocity while an inverse relationship with heat transfer. Consequently, as the amount of Ec escalations, the fluidity intensifies, while the HT rate decreases, resulting in a decrease in the value ofN_n.

It is indeed intriguing to observe that the initial solution experiences a decline, whereas the subsequent solution undergoes an increment. Moreover, mixed outline is pragmatic for the second branch. In the range $0.2 \le Pr \le 0.7$, the Nusselt number surges whereas in the range $0.7 < Pr \le 0.8$, the TH rate develops. Also, the Nusselt number decays when the level of Q (sink or source) are enhanced.

Figures 10-14 delve into the investigation of the fluctuation of the HNF velocity profile$f'(\eta)$, taking into consideration various influential parameters such as $B, Gr, Gm, M,$ and K. Figure 10 specifically focuses on the impact of B on fluid movement. Through a meticulous analysis of this figure, it has been observed that dual solutions have emerged as a result of the shrinking occurrences. It is crucial to note that the fluid motion experiences a decline as the amount of B are augmented. Moreover, it is intriguing to declaration at this juncture that the dominance of the first solution in comparison to the second solution is attributable to the intricate connection between the heat at the surface and the surrounding liquid. As the strengthening of B occurs, the aforementioned correlation becomes more significant, which in turn leads to a noticeable decrease in the value of $f'(\eta)$ within the specified range $0 \le \eta \le 2.5$. Graphs 11 and 12 delve into the examination of the correlation between the HNF velocity and the Grashof number (Gr) and modified Grashof number(Gm). It is noteworthy to highlight that the similar influence is detected for both factors, meaning that the velocity of the HNF experiences an escalation as the values of Gr and Gm increase. Taking into account both cases, it becomes evident that the velocity of the second branch surpasses than first. The Grashof number serves as a tool for comprehending the relationship between the dynamics of viscosity and the thermal buoyancy force, while the Gm serves as a means to identify the connection between the dynamics of viscosity and the buoyancy force related to the species being transferred. Thus, by increasing

these factors, not only does the thermal buoyancy force rise but also the mass buoyancy force experiences an upsurge. Figures 13 and 14, on the other hand, aim to examine the variations of the M parameter and K factors on $f'(\eta)$. The investigation of diminishing performance is conducted for both velocities as the value of M, is enhanced. It is important to note that the profile $f'(\eta)$, which characterizes the fluid flow, displays a growing tendency with reverence to the parameter$K$. As the level of M is augmented from 0.1 to 1, an interesting phenomenon occurs with the Lorentz force resulting from the presence of a magnetic field. This force acts as a hindrance to the gesture of the fluid particles, leading to a deterioration in the fluid movement and a reduction in the depth of the boundary layer. This observation is depicted in Figure 14, where it is clearly demonstrated that the fluid motion intensifies as the values of the porosity factor increase within the range of 1 to 1.9. From a physical standpoint, the increase in the quantities of K causes the holes in the sheet to enlarge, thus facilitating a greater influx of fluid inside the sheet. Consequently, the motion of the fluid molecules becomes accelerated, resulting in a faster overall fluid motion.

Figures 15-18 delve into the examination of the effects of $R, Q, Q1$, and Pr on the temperature of HNF. Figure 15 presents a graphical representation of the relationship between the temperature and the radiation factor$R$. Through this comprehensive analysis, it is elucidated that temperature exhibits a direct proportionality to$R$, meaning that when R increases, temperature also experiences an improvement in its value. This augmentation in temperature is accompanied by an upsurge in the depth of the boundary layer. The rationale behind this phenomenon lies in the fact that as the radiation factor enhances from 0.1 to 0.7, more heat is transmitted to the HNF, leading to an upsurge in its temperature. Furthermore, the thermal diffusion process is significantly enhanced as a result of the larger quantities of R present, which in turn governs the enhancement of the fluid temperature of the HNF. It is important to note that this increasing trend is observed for both solutions. Upon analyzing Figures 16 and 17, it is discerned that temperature experiences a growth pattern in relation to Q and$Q1$, respectively, within the range of 0.1 to 0.7. This physical occurrence can be ascribed to the absorption (generation) of heat which happens in the warm area, as the values of Q and $Q1$ persistently improve. The occurrence of an unusually high quantity of intensity within the liquid serves to stimulate the enhancement of atomic power within the HNF. This, in turn, leads to the upsurge of the BLT (Boundary Layer Thickness) and consequently facilitates the transport of heat energy, thereby significantly

improving the temperature of the system. In order to investigate the stimulus of the Pr (Prandtl number) on heat of the HNF, a schematic representation, denoted as Figure 18, has been devised. The phenomenon of thermal radiation can be understood as the ratio between the thermal diffusivity and the momentum diffusivity. With an upsurge in Pr, there is an accompanying decrease in both the thermal diffusivity and the heat dissipation, albeit to a slight extent. As a result, the heat rate experiences a minor enhancement, leading to a rapid decline in heat of the HNF, as exemplified in graph 18.

Figures 19-21 visually depict the influence of $Ec, Du,$ and Sr on the distribution of temperature and concentration. In the case ofEc, Figure 19 delves into the relationship between Ec and profiles temperature and concentration. This analysis reveals the existence of dual solutions for both temperature and concentration when Ec serves as the driving force. It is noteworthy that an increasing trend is observed in both profiles as the Ec values are augmented from 0.1 to 1. It is intriguing to observe that the variation in the second solution surpasses that of the first. From a physical standpoint, when the magnitude of Ec is heightened, the mechanical energy experiences a rapid transformation into thermal energy, thereby remarkably enhancing the temperature of the HNF throughout the entire channel. The growth of Ec indicates a rise in the conversion of mechanical energy into thermal energy, resulting in an overall elevation in temperature. Correspondingly, the influence of Du on the fluctuations of temperature and concentration is depicted in graph 20. The performance exhibited by Du regarding temperature and concentration is witnessed as deliberated in graph 19 forEc. The disparity in temperature is found to be further noteworthy than concentration. The temperature increase is directly correlated to the intensity of Du because of its influence on the thermal slopes of concentration inside the liquid. Hence, higher amount of Du result in an augmentation of temperature and the depth of the thermal BL. Figure 21 delves into the examination of the impact of Sr on the fluctuations in temperature and concentration. This all-encompassing examination demonstrates that the augmentation in Sr leads to a simultaneous increase in both temperature and concentration. It is pragmatic that as the magnitude of Sr elevates from 0.1 to 0.4, there is a notable escalation in NHF temperature as well as concentration. Furthermore, it is wealth mentioning that the rise in heat is deemed to be more significant in comparison to concentration for both branches of solutions. This can be accredited to the emergence of a substantial mass diffusivity phenomenon, which is only manifested when Sr is heightened from 0.1 to 0.4.

6. Conclusions

The main aim of the current investigation is to scrutinize the phenomenon of cross-diffusion of magnetized HNF above an elongated or contracting surface in the incidence of thermal conductivity. In imperative to assess the stability of the scheme, the eigenvalues are computed. It is noteworthy that the existence of the smallest positive eigenvalues signifies the presence of stable solutions, whereas the negative eigenvalues indicate the existence of unstable solutions. The mathematical representation of the flow models is transformed into ODEs via resemblance transformations. The statistical outcomes are achieved by employing the bvp4c technique. To provide a comprehensive understanding of the physical factors governing fluid dynamics, the graphical and tabular representations are utilized to elaborate upon the inspiration behind these factors. This finding was reported by Dero et al. [30] and has since been supported by numerous studies in the field. The importance of conducting a stability analysis cannot be overstated, as it allows researchers to understand the behavior of a system when duality arise.

1. In particular, dual variation is often witnessed for the factors B and M on S_f. This dual fluctuation phenomenon is characterized by an increase in S_f in the first branch and a subsequent decrease in S_f in the second branch.
2. Moreover, it has been observed that as the amount of M increase from 1 to 3, S_f also boosts. Also, when the parameter B is increased from 1 to 5, S_f exhibits a corresponding rise. These findings suggest a positive relationship between M, B and S_f. However, it is important to note that the relationship between S_f and other variables, such as Gr and M is more complex.
3. In fact, it has been investigated that S_f tends to decrease as the quantities of Gr and M are enlarged for both both of the hybrid NF model. This finding highlights the intricate interplay between various parameters and their impact on the stability of the system.
4. It is widely acknowledged that as the magnitude of Du increases from 1 to 3, there is a discernible reduction in the HT rate in HNF. In the context of fluid dynamics, it has been determined that the fluid velocity experiences a decline when the values of variable B are enhanced.

5. By analyzing the behavior of the velocity branches, it becomes evident that both branches exhibit a decreasing trend as the M is improved. On the other hand, the velocity profile displays a growing trend with respect to variable$K$. This increasing trend suggests that the variation in velocity is positively influenced by the values of variable K varying from 1 to 1.9.
6. Furthermore, a comprehensive analysis of the temperature variable reveals that it is directly proportional to the variable$R$. This direct proportionality suggests that as the variable R increases, the temperature also increases.
7. Additionally, it has been reported that the temperature is a growing function of variables Q and $Q1$, with values ranging from 0.1 to 0.7. This growing function implies that as the values of Q and $Q1$upturn within the specified range, the temperature also exhibits an upward trend.
8. Similarly, an increasing phenomenon has been reported for the temperature and concentration profiles as the amounts of variable Ec are improved from 0.1 to 1.

   Theoretical analysis's conclusions have important ramifications for many industries, comprising technology, automobile solar thermal and cooling systems, lubricating properties, hybrid power plants, metallic welding procedures, and healthcare product manufacturing. These applications underscore the results' practical value and their potential influence on a wide range of sectors.

Conflict of interest: No conflict of interest exists about this manuscript.

Data availability: All the data exist within the manuscript.

Authors contribution statement: Conceptualization, A.M.M. and Zeeshan.; methodology, Zeeshan and M.A.; software, Zeeshan, N.I.; validation, A.M.M, N.I. and Zeeshan.; formal analysis, Zeeshan, A.M.M.; investigation, Zeeshan, R.S, and Zeeshan.; writing—original draft preparation, A.M.M. and N.I.; writing—review and editing, Zeeshan, A.M.M, R.S. and Zeeshan; visualization. All authors have read and agreed to the published version of the manuscript.

Author's biographies

Ali M. Mahnashi is an Assistant Professor in the Department of Mathematics at the College of Science, Jazan University, Jazan, Saudi Arabia. His expertise lies in the fields of applied mathematics, where he has made significant contributions through numerous publications in high-impact factor journals. His research focuses on advancing mathematical methods and their applications, enhancing the understanding of statistical models, and contributing to various scientific disciplines. His work has earned him recognition within the academic community, underscoring his role in the development of statistical theory, data analysis and its practical implementations.

Dr. Zeeshan earned his M.Sc. and M.phil degree from Quaid-e-Azam University, Islamabad and the Ph.D. degree from Abdul Wali Khan University, Mardan, KP, Pakistan. He is currently an Assistant Professor in mathematics with Bacha Khan University Charsadda, KP, and Pakistan. He has published 90 articles in good impact factor journals and has participated in national conference. His research interests include magnetohydrodynamic, nano fluid, heat transfer, Hall Effect, electrohydrodynamic, thin film, and heat exchangers.

Mohammad Alqudah is an AssociateProfessor in the Department of Basic Sciences at German Jordanian University where he has been a faculty member since September 2015. Dr. AlQudah has been teaching mathematics for the past 16 years, most recently as an Assistant Professor in the Department of Mathematics and Statistics at Northwood University-Michigan, USA where he has been a faculty member from January 2011-September 2015. He was the Chairperson of Department of Mathematics at Northwood University, and held the position from June 2011-Sept 2015. Dr. AlQudah is a Project NExT fellow from the Michigan Section of the MAA since 2012.

His research interests lie in the area of Approximation of vector valued functions by polynomials with coefficients in vector spaces. Recently, he has focused on construct classical and generalized orthogonal polynomials with respect to some weight functions.

Naveed Iqbal is serving as an Associate Professor at Department of Mathematics, College of Science, University of Ha'il, Saudi Arabia. He has done BS(Hons) in 2012 from Kohat University of Science and Technology, Kohat, Pakistan. He received M.Phil. degree in 2014 (National University of Science and Technology, Islamabad, Pakistan). He has done his Ph.D. in 2019 (School of Mathematical Sciences, Anhui University, Hefei, China). He has authored over 88 papers in various journals. His research interests are in the field of dynamical systems, mathematical biology, CFD, and numerical analysis.

Rasool Shah completed PhD at Abdul Wali Khan University, Mardan, Pakistan, in 2020. He has currently a postdoctoral researcher at the Lebanese American University, Beirut, Lebanon. To date, have published 190 papers in journals with significant impact factors, contributing to advancements in applied mathematics and computational techniques.

References

[1] Etemad S.G., Farajollahi B., Hajipour M. and Thibault. "Turbulent convective heat transfer of suspensions of γ-Al 2 O 3 and CuO nanoparticles (nanofluids)", *Journal of Enhanced Heat Transfer*, 19(3) (2012). DOI: 10.1615/JEnhHeatTransf.2012000620

[2] Bég O.A. and Tripathi D. "Mathematica simulation of peristaltic pumping with double-diffusive convection in nanofluids: a bio-nano-engineering model. Proceedings of the Institution of Mechanical Engineers", *Part N: Journal of Nanoengineering and Nanosystems*, 225(3), pp.99-114 (2011). DOI:10.1177/1740349912437087

[3] Bég O.A., Bég T.A., Rashidi M.M., et al. "DTM-Padé semi-numerical simulation of nanofluid transport in porous media", *International Journal of Applied Mathematics and Mechanics*, 9, pp.80-107 (2013). doi.org/10.1016/j.icheatmasstransfer.2020.105085

[4] Rana P., Bhargava R. and Bég O.A. "Numerical solution for mixed convection boundary layer flow of a nanofluid along an inclined plate embedded in a porous medium", *Computers and Mathematics with Applications*, 64(9), pp.2816-2832 (2012). doi.org/10.1016/j.camwa.2012.04.014

[5] Bég O.A., Bég T.A., Rashidi M.M., et al. "Homotopy semi-numerical modelling of nanofluid convection boundary layers from an isothermal spherical body in a permeable regime", *International Journal of Microscale and Nanoscale Thermal Fluid Transport Phenomena*, 3, pp.237-266 (2012). doi.org/10.3390/inventions4040054

[6] Rashidi M.M., Bég A.O., Freidooni M.N., et al. "Homotopy simulation of axisymmetric laminar mixed convection nanofluid boundary layer flow over a vertical cylinder", *Theoretical and Applied Mechanics*, 39(4), pp.365-390 (2012). DOI:10.2298/TAM1204365R

[7] Muneeshwaran M., Srinivasan G., Muthukumar P., et al. "Role of hybrid-nanofluid in heat transfer enhancement–A review", *International Communications in Heat and Mass Transfer*, 125, p.105341 (2021). doi.org/10.1016/j.icheatmasstransfer.2021.105341

[8] Kshirsagar D.P. and Venkatesh M.A. "A review on hybrid nanofluids for engineering applications", *Materials Today: Proceedings*, 44, pp.744-755 (2021). doi.org/10.1016/j.matpr.2020.10.637

[9] Esfe M.H., Bahiraei M. and Mir A. "Application of conventional and hybrid nanofluids in different machining processes: A critical review", *Advances in Colloid and Interface science*, 282, p.102199 (2020). doi.org/10.1016/j.cis.2020.102199

[9] Satya Narayana P.V., Venkateswarlu B. and Venkataramana S. "Thermal radiation and heat source effects on a MHD nanofluid past a vertical plate in a rotating system with porous medium", *Heat Transfer—Asian Research*, 44(1), pp.1-19 (2015). doi.org/10.1002/htj.21101

[10] Satya Narayana P.V. and Venkateswarlu B. "Influence of variable thermal conductivity on MHD casson fluid flow over a stretching sheet with viscous dissipation, Soret and Dufour Effects", *Frontiers in Heat and Mass Transfer*, 7(1) (2016). doi.org/10.5098/hmt.7.16

[11] Adun H., Wole-Osho I., Okonkwo E.C., et al. “A critical review of specific heat capacity of hybrid nanofluids for thermal energy applications”, *Journal of Molecular Liquids*, 340, p.116890 (2021). doi.org/10.1016/j.molliq.2021.116890

[12] Akilu S., Baheta A.T., Said M.A.M., et al. “Properties of glycerol and ethylene glycol mixture based SiO2-CuO/C hybrid nanofluid for enhanced solar energy transport”, *Solar Energy Materials and Solar Cells*, 179, pp.118-128 (2018). doi.org/10.1016/j.solmat.2017.10.027

[13] Ashorynejad H.R. and Shahriari A. MHD natural convection of hybrid nanofluid in an open wavy cavity. Results in Physics, 9, pp.440-455 (2018). doi.org/10.1016/j.rinp.2018.02.045

[14] Aziz A. “A similarity solution for laminar thermal boundary layer over a flat plate with a convective surface boundary condition”, *Communications in Nonlinear Science and Numerical Simulation*, 14(4), pp.1064-1068 (2009). doi.org/10.1016/j.cnsns.2008.05.003

[15] Yao S., Fang T. and Zhong Y. “Heat transfer of a generalized stretching/shrinking wall problem with convective boundary conditions”, *Communications in Nonlinear science and Numerical simulation*, 16(2), pp.752-760 (2011). doi.org/10.1016/j.cnsns.2010.05.028

[16] Temimi H., Ben-Romdhane M., Ansari A.R., et al. “Finite difference numerical solution of troesch’s problem on a piecewise uniform shishkin mesh”, *Calcolo*, 54(1), pp.225-242 (2017). DOI 10.1007/s10092-016-0184-1. DOI 10.1007/s10092-016-0184-1

[17] Ben-Romdhane, M. and Temimi H. “An iterative numerical method for solving the Lane–Emden initial and boundary value problems”, *International Journal of Computational Methods*, 15(04), p.1850020 (2018). doi.org/10.1142/S0219876218500202

[18] Temimi H. and Ben-Romdhane M. “Numerical solution of Falkner-Skan equation by iterative transformation method”, *Mathematical Modelling and Analysis*, 23(1), pp.139-151 (2018). doi.org/10.3846/mma.2018.009.

[19] Temimi H., Ben-Romdhane M., Baccouch M., et al. “A two-branched numerical solution of the two-dimensional Bratu's problem”, *Applied Numerical Mathematics*, 153, pp.202-216 (2020). doi.org/10.1016/j.apnum.2020.02.010

[20] Chaudhary M.A. and Merkin J.H. “A simple isothermal model for homogeneous-heterogeneous reactions in boundary-layer flow in equal diffusivities”, *Fluid dynamics research*, 16(6), pp.311-333 (1995). doi.org/10.1016/0169-5983(95)00015-6

[21] Kumar A. and Yadav P.K. “Heat and mass transfer analysis for MHD non-miscible micropolar and Newtonian fluid flow in a rectangular porous channel”, *ZAMM-Journal of Applied Mathematics and Mechanics/Zeitschrift für Angewandte Mathematik und Mechanik*, 103(12), p.e202200589 (2023). doi.org/10.1002/zamm.202200589

[22] Yadav P.K. and Yadav N. “Impact of heat and mass transfer on the magnetohydrodynamic two-phase flow of couple stress fluids through a porous walled curved channel using homotopy

analysis method", *Chaos, Solitons & Fractals*, 183, p.114961 (2024). DOI: 10.1016/j.chaos.2024.114961

[23] Yadav P.K., and Srivastava P. "Impact of porous material and slip condition on the MHD flow of immiscible Couple stress-Newtonian fluids through an inclined channel: Head loss and pressure difference", *Chinese Journal of Physics*, 89, pp.1198-1221 (2024). doi.org/10.1016/j.cjph.2024.03.046

[24] Jaiswal S. and Yadav P.K. "Flow of micropolar–Newtonian fluids through the composite porous layered channel with movable interfaces", *Arabian Journal for Science and Engineering*, 45(2), pp.921-934 (2020). DOI:10.1007/s13369-019-04157-2

[25] Yadav P.K., Jaiswal S., Puchakatla J.Y., et al. "Poiseuille flow of micropolar-Newtonian fluid through concentric pipes filled with porous medium", *Colloid Journal*, 82, pp.333-341 (2020). DOI: 10.1134/S1061933X20030047

[26] Makinde O.D., Zimba K. and Bég O.A. "Numerical study of chemically-reacting hydromagnetic boundary layer flow with Soret/Dufour effects and a convective surface boundary condition", *International Journal of Thermal and Environmental Engineering*, 4(1), pp.89-98 (2012). DOI:10.5383/ijtee.04.01.013

[27] Manjunatha S., Kuttan B.A., Jayanthi S., et al. "Heat transfer enhancement in the boundary layer flow of hybrid nanofluids due to variable viscosity and natural convection", *Heliyon*, 5(4) (2019). doi.org/10.1016/j.heliyon.2019.e01469

[28] Venkateswarlu B., and Satya Narayana P.V. "Cu-Al2O3/H2O hybrid nanofluid flow past a porous stretching sheet due to temperatue-dependent viscosity and viscous dissipation", *Heat Transfer*, 50(1), pp.432-449 (2021). doi.org/10.1002/htj.21884

[29] Lund L.A., Omar Z., Khan, I., et al. "Magnetohydrodynamic (MHD) flow of micropolar fluid with effects of viscous dissipation and joule heating over an exponential shrinking sheet: triple solutions and stability analysis", *Symmetry*, 12(1), p.142 (2020). doi.org/10.3390/sym12010142

[30] Dero S., Rohni A.M. and Saaban A. "Stability analysis of C u− C 6 H 9 N a O 7 and Ag− C 6 H 9 Na O 7 nanofluids with effect of viscous dissipation over stretching and shrinking surfaces using a single phase model", *Heliyon*, 6(3) (2020). doi.org/10.1016/j.heliyon.2020.e03510

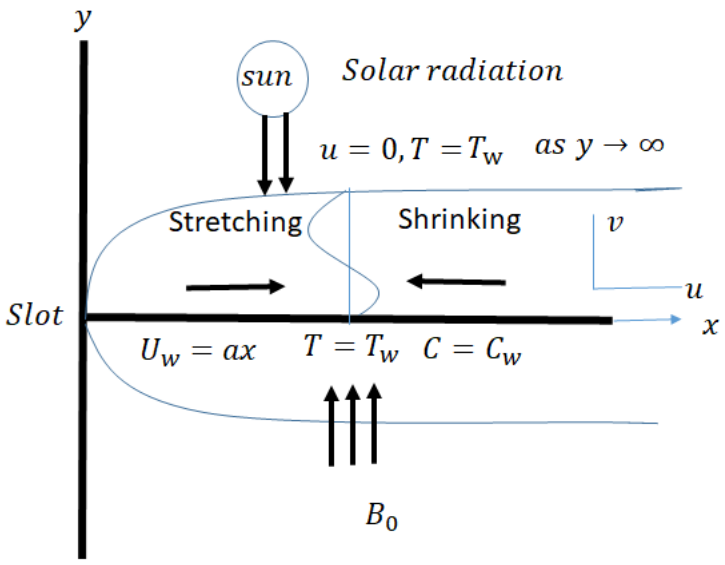

Fig. 1. Flow geometry.

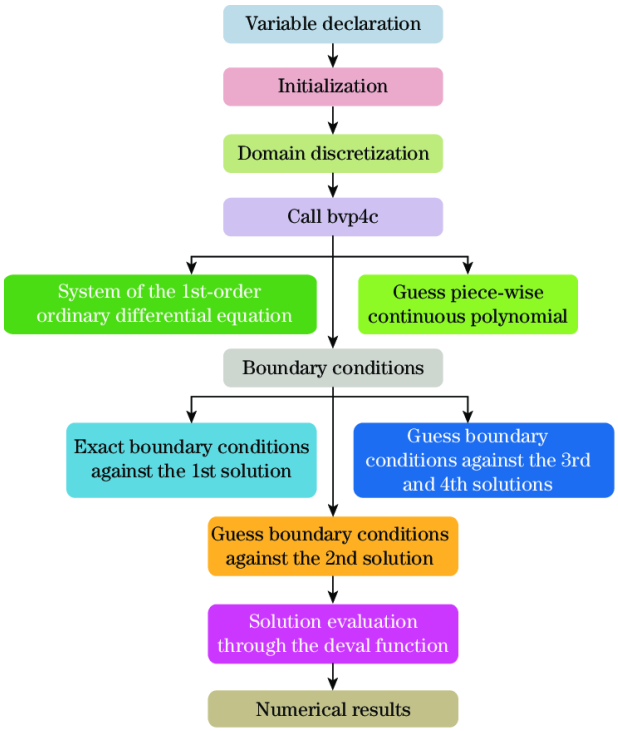

Fig. 2. bvp4c procedure.

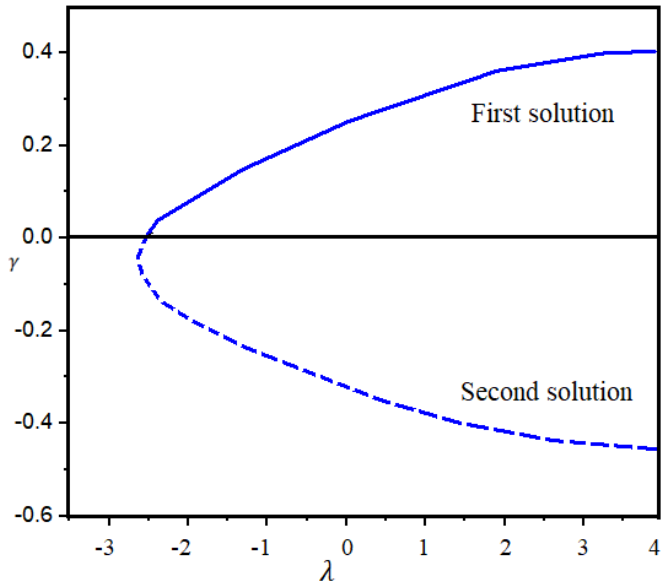

Fig. 3. Stable and unstable solutions presentation.

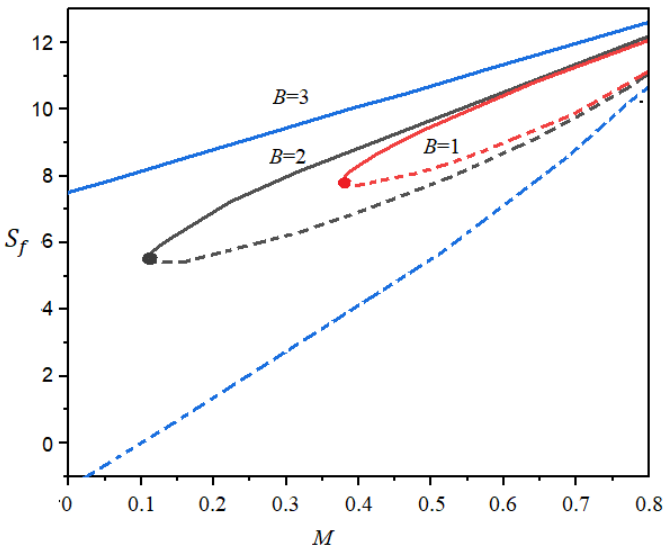

Figure 4. Scattering of S_f regarding B and M.

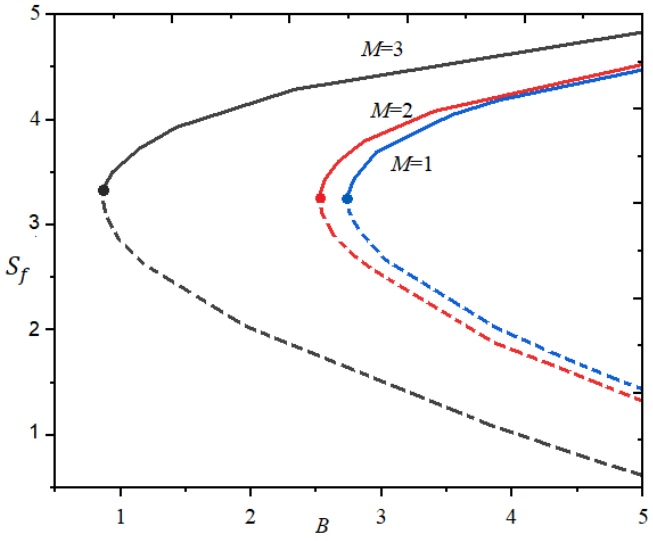

Figure 5. Scattering of S_f regarding M and B.

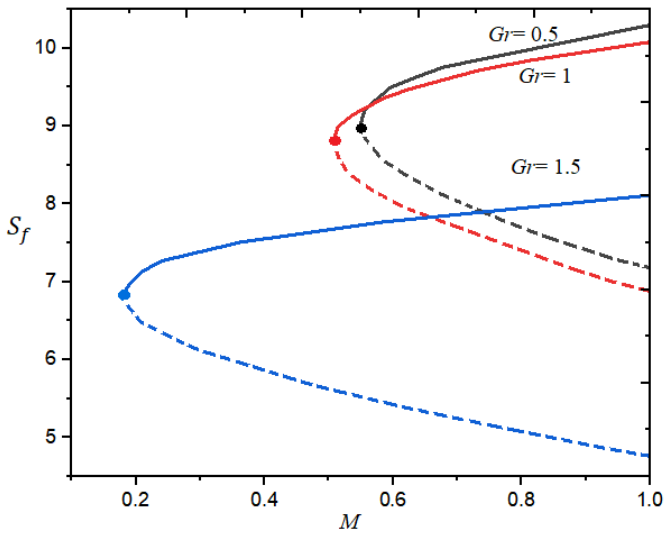

Figure 6. Scattering of S_f regarding M and Gr.

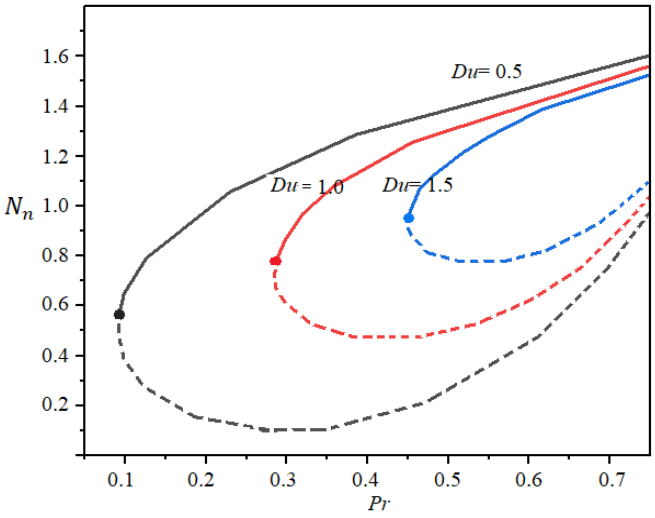

Figure 7. Distribution of N_n regarding Du and Pr.

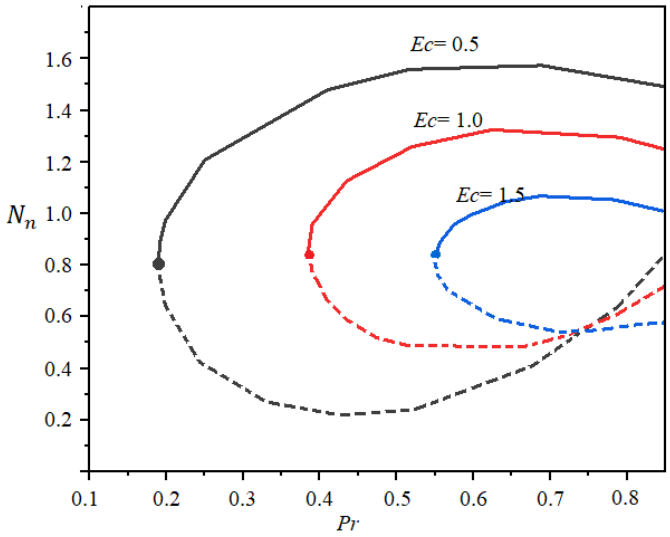

Figure 8. Distribution of N_n regarding Ec and Pr.

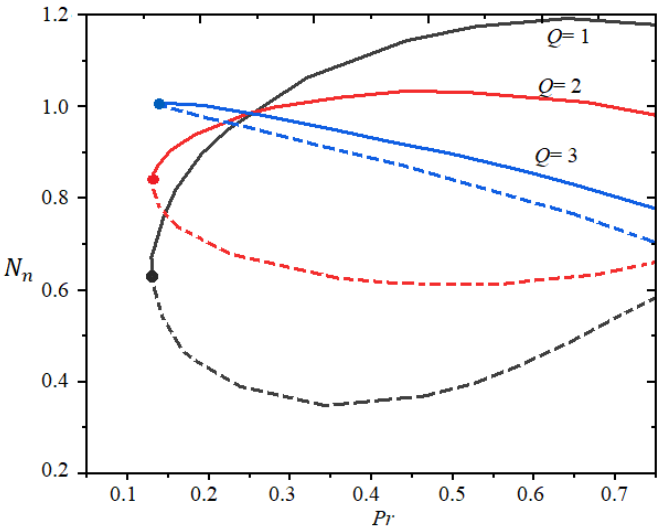

Figure 9. Distribution of N_n regarding Q andPr.

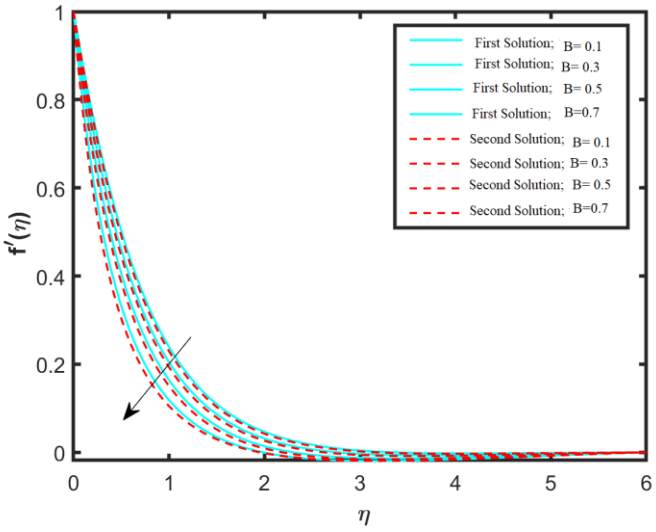

Figure 10. Inspiration of B on $f'(\eta)$.

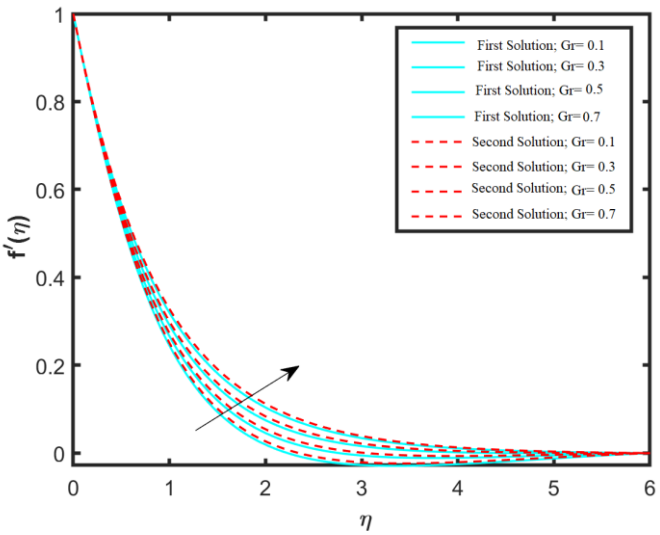

Figure 11. Inspiration of Gr on $f'(\eta)$.

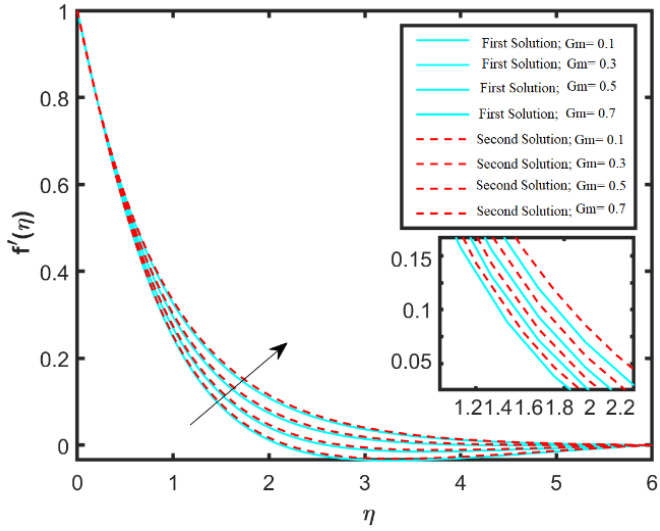

Figure 12. Inspiration of Gm on $f'(\eta)$.

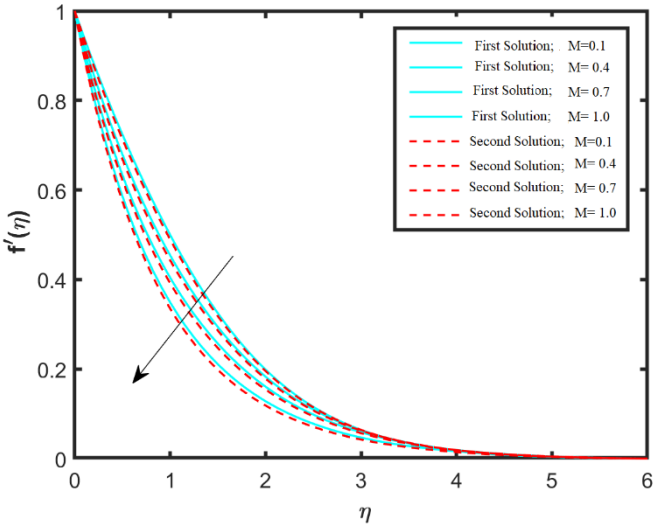

Figure 13. Inspiration of M on $f'(\eta)$.

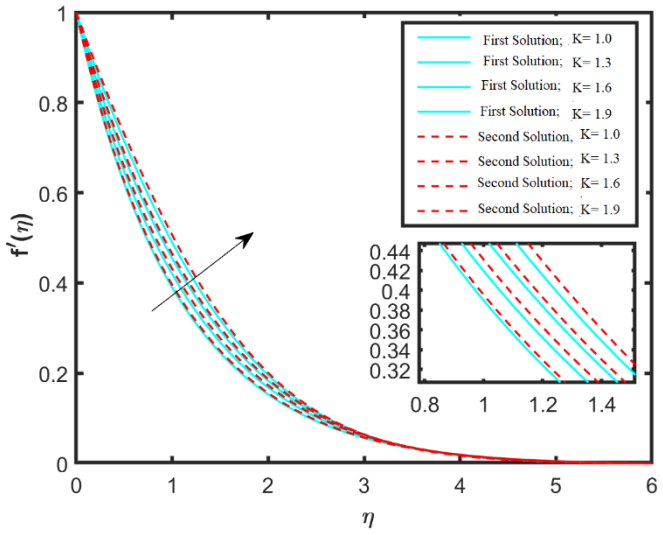

Figure 14. Inspiration of K on $f'(\eta)$.

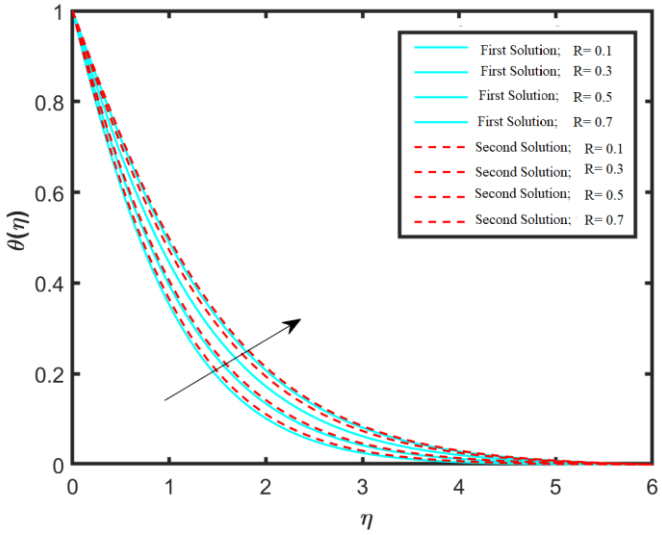

Figure 15. Inspiration of R on $\theta(\eta)$.

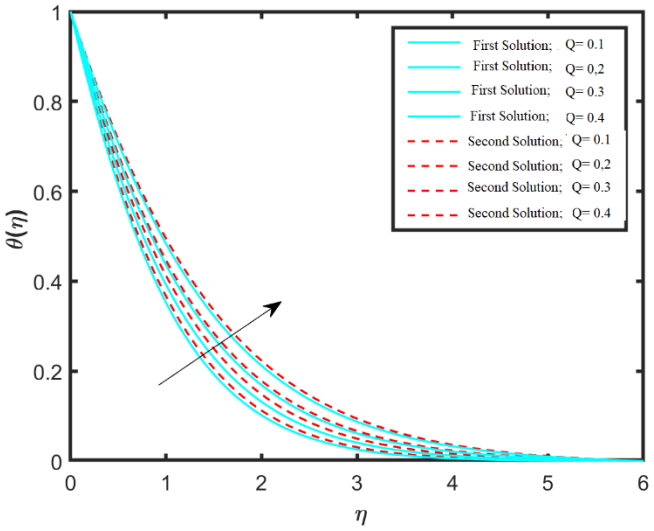

Figure 16. Inspiration of Q on $\theta(\eta)$.

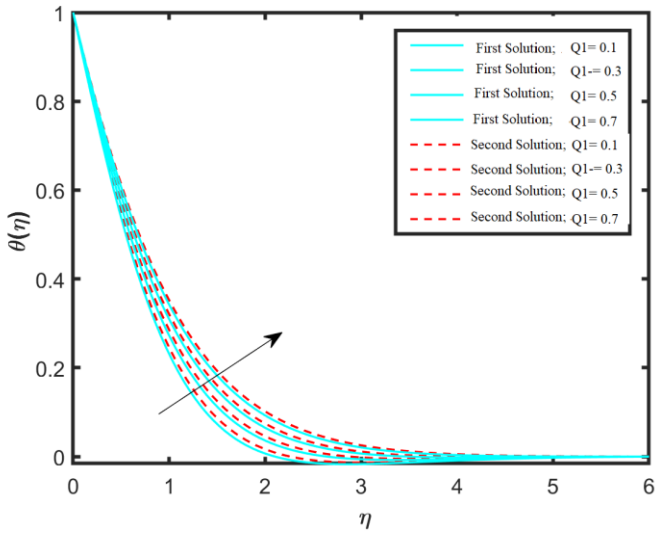

Figure 17. Inspiration of $Q1$ on $\theta(\eta)$.

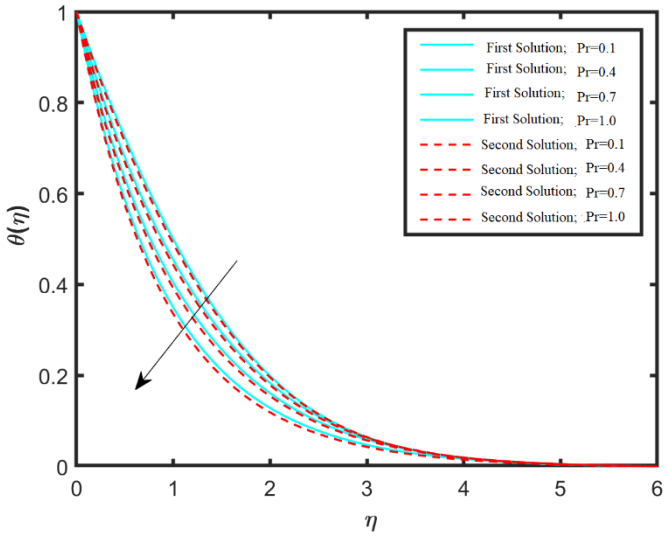

Figure 18. Inspiration of Pr on $\theta(\eta)$.

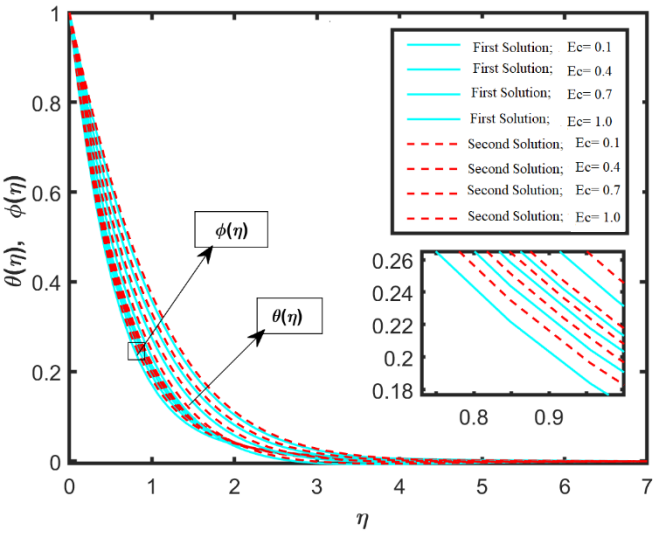

Figure 19. Inspiration of Ec on $\theta(\eta)$ and $\phi(\eta)$.

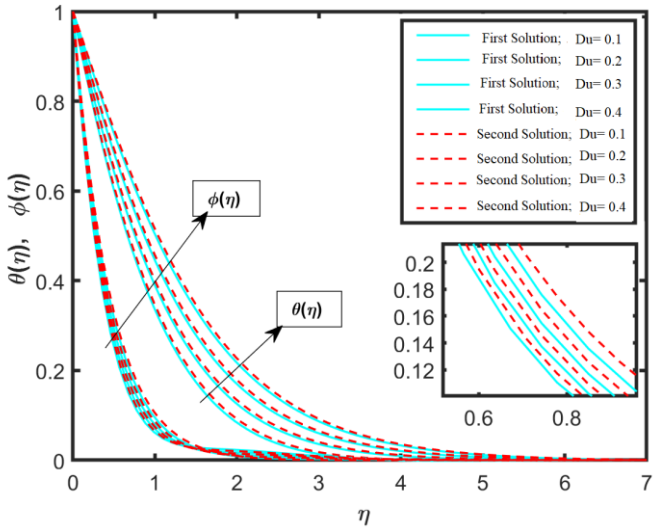

Figure 20. Inspiration of Du on (η) and $\phi(\eta)$.

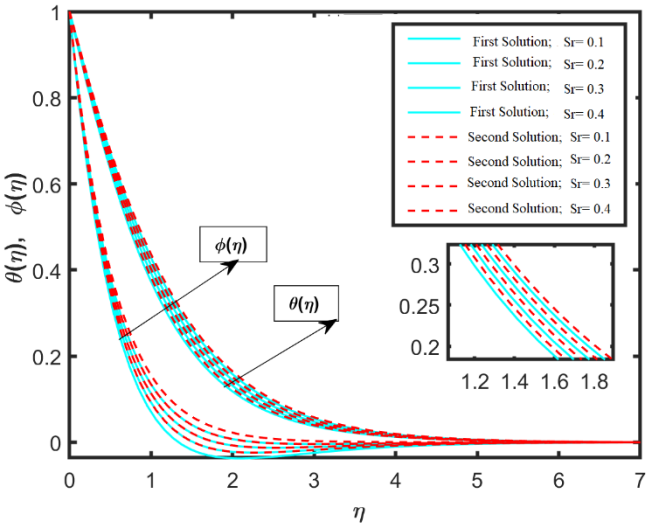

Figure 21. Inspiration of Sr on $\theta(\eta)$ and $\phi(\eta)$.

Table 1. Physical properties of H_2O , Al_2O_3, and Cu [27, 28].

Thermal physical properties	Al_2O_3	Cu	Base fluid H_2O
Density $(\rho)(kgm^{-3})$	3,9770	8,933	997.1
Thermal expansion coefficient $(\beta \times 10^{-5})(K^{-1})$	5.1	76.5	25.6
Thermal conductivity $(k)(Wm^{-1}\ K^{-1})$	40	400	0.6071
Heat capacity $(C_p)(Jkg^{-1}\ K^{-1})$	765	385	4,179

Table 2. Thermo-physical properties of HNFs and NFs [27, 28].

Thermal physical properties	HNFs $(Cu - Al_2O_3: H_2O)$	NFs $(Cu: H_2O)$
μ	$\mu_{hnf} = \mu_f(1-\phi_1)^{-2.5}(1-\phi_2)^{-2.5}$	$\mu_{nf} = \mu_f(1-\phi_2)^{-2.5}$
ρ	$\rho_{hnf} = \phi_2\rho_{s2}\{(1-\phi_1)\rho_f + \phi_1\rho_{s1}\} + \phi_2\rho_{s2}$	$\rho_{nf} = (1-\phi_2)\rho_f + \phi_2\rho_{s2}$
β	$\beta_{hnf} = \phi_2\beta_{s2}\{(1-\phi_1)\beta_f + \phi_1\beta_{s1}\} + \phi_2\beta_{s2}$	$\beta_{nf} = (1-\phi_2)\beta_f + \phi_2\beta_{s2}$
C_p	$(\rho C_p)_{hnf} = \phi_2(\rho C_p)_{s2} + (1-\phi_2)(\rho C_p)_{s2}$ $\{(1-\phi_1)(\rho C_p)_f + \phi_1(\rho C_p)_{s1}\}$	$(\rho C_p)_{nf} = (1-\phi_2)(\rho C_p)_f + \phi_2(\rho C_p)_{s2}$
k	$\frac{k_{hnf}}{k_{bf}} = \frac{k_{s1} + (n-1)\{k_{hf} + \phi_1(k_{s1} - k_f)\}}{k_{s1} + (n-1)\{k_{bf} + \phi_1(k_f - k_{s1})\}}$	$\frac{k_{nf}}{k_f} = \frac{k_{s2} + (n-1)\{k_f + \phi_2(k_{s2} - k_f)\}}{k_{s2} + (n-1)\{k_f + \phi_2(k_f - k_{s2})\}}$

Table 3. Validation table for SDF [27, 28].

M & B	SDF					
	[27]		[28]		Recent study	
	$Cu - H_2O$	$Cu - Al_2O_3 - H_2O$	$Cu - H_2O$	$Cu - Al_2O_3 - H_2O$	$Cu - H_2O$	$Cu - Al_2O_3 - H_2O$
0.3	0.5070	0.5005	0.50714	0.50142	0.507107	0.500426
0.6	0.5545	0.5584	0.55467	0.55930	0.554603	0.558382
0.9	0.6010	0.6142	0.60112	0.61518	0.601160	0.614102
1.5	0.6465	0.6680	0.64664	0.66894	0.646665	0.668310
2.0	0.6910	0.7199	0.69217	0.72925	0.691100	0.719205
2.5	0.7504	0.7961	0.75192	0.81063	0.7501031	0.796038
3.0	0.8146	0.8794	0.81665	0.90014	0.814503	0.879341
3.5	0.8838	0.9699	0.88641	0.99762	0.883514	0.968826

Table 4. Validation table for Nusselt number using various quantities of Pr.

Pr	Nusselt number					
	[27]		[28]		Recent study	
	$Cu - H_2O$	$Cu - Al_2O_3 - H_2O$	$Cu - H_2O$	$Cu - Al_2O_3 - H_2O$	$Cu - H_2O$	$Cu - Al_2O_3 - H_2O$
0.7	0.2037	0.2064	0.20198	0.20582	0.203620	0.206261
1.2	0.2014	0.2128	0.20185	0.21694	0.201372	0.215536
1.5	0.2021	0.2192	0.20273	0.21885	0.202174	0.218904
2.2	0.2027	0.2257	0.20269	0.22727	0.203053	0.226425